A Study of the Potentiality of Inkjet-Printing Technique for the Fabrication of Metal-Insulator-Semiconductor Organic Rectifying Diodes

Silvia Conti; Carme Martinez-Domingo; Lluís Terés; Eloi Ramon; Institut de Microelectrónica de Barcelona, IMB-CNM (CSIC), Cerdanyola del Vallès, Catalonia, Spain

Abstract

A route for the inkjet-printing of organic rectifying diodes based on Metal-Insulator-Semiconductor (MIS) structure is outlined. The proposed strategy is based on a layer stack of two silver electrodes between which a polyvinyl phenol (PVP) insulator layer and an amorphous organic semiconducting layer are sandwiched. Thanks to the energy barrier given by the presence of a leaky dielectric layer between the electrode and the semiconductor, the current versus voltage characteristics present a rectification ratio of up to $1.5*10^3$ at $|10\ V|$ and a current density up to approximately $0.1 mAcm^{-2}$. Finally, a first example of a gas sensor based on the MIS diode is presented as a proof-of-concept for the possible applications of these structures.

Introduction

Printed Electronics (PE) is one of the fastest growing technologies in the world and an emerging industry that takes advantage of conventional Graphic Art Printing (GAP) approaches to manufacture low-cost, high-volume and high-throughput electronic and optoelectronic devices that are light-weight, thin, flexible, and potentially disposable on plastic, paper, conformable, and transparent substrates. This evolution is being delivered principally through adaptations of the device fabrication technologies, increasing throughputs, decreasing feature sizes, and driving production costs down. [1] With the increasing ambition to commercialize low-cost electronic platforms, inkjet-printing has become one of the most promising among the various printing techniques thanks to it being a versatile, additive, mask-less, low-material, low-time, and low-power consuming approach. [2],[3] The potential applications of this technique could be endless, and several works have been reported both for single-layer printed structures as well as for multilayer stacks. [4]-[7] However, the use of inkjet-printing technique as the only fabrication process, even for a simple electronic device, e.g. a diode, is still a challenge. The key component of a diode is the junction that permits the current to flow in one direction but not in another. Most of the work has been focused on the fabrication of organic Schottky diodes. These devices are, generally, based on the misalignment of the Work Functions (WFs) of the anode and cathode electrodes, and, as a consequence, on the employment of two different metals to form the potential energy barrier (Schottky Barrier Height, SBH) responsible of the rectifying behavior. [8] However, p-type Organic Semiconductors (p-OSCs) usually have Highest Occupied Molecular Orbital (HOMO) levels in the same range of the WFs of the most common printable metals. For this reason, ohmic contacts between the metals and the semiconductor are expected. [9] This issue can be overcome exploiting the rectifying behavior of Metal-Insulator-Semiconductor (MIS) structures in which the blocking energy barrier is given by the insertion of a leaky insulator between the metal and the semiconductors layers, as recently observed in [10]-[11]. In this way, there is no need to have rectifying electrodes with misaligned WFs.

In this paper, MIS organic rectifying diodes fabricated using a multi-nozzle inkjet-printing system are reported. A reliable process for the deposition of the two polymeric films is established as a key factor for obtaining high performance devices. To this aim, different formulations and deposition processes are investigated. Morphological and electrical characterizations are provided in order to understand the performances of the presented diodes.

Results and Discussion

Figure 1 shows the scheme and the optical image of the MIS organic diodes. All the structures were fabricated on Polyethylene naphthalene (PEN) substrates. Inkjet-printing was employed for the patterning of the bottom electrode (silver(p)) and the insulator. The top electrode (silver(f)) was deposited by drop casting using a silver flake ink. In the devices referred as *MIS* the semiconductor was drop-casted, whilst in the devices referred as *MISp* the semiconductor was inkjet-printed.
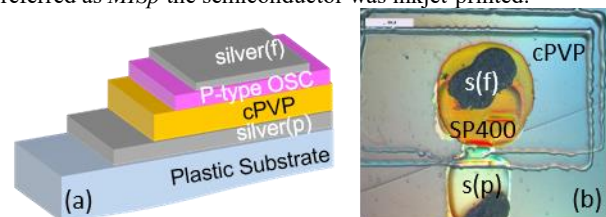
Figure 1 Scheme (a) and optical image (b) of MIS structure.

All the materials were selected considering their different role in the electrical behavior of the diodes. As far as the electrodes are concerned, a large number of conductive inks, based on silver, copper, or poly(3,4-ethylenedioxythiophene) polystyrene sulfonate are available for printing processes. All of these conductors present WFs that depend strongly on their oxidation states, [12] and their doping states [13]. This can lead to high WF values due to uncontrolled variations of the energy levels. Kelvin Probe Force Microscopy (KPFM) measurements of the silver electrodes used in this work gave WFs of around $\Phi M=-5.2eV$. As already underlined in the introduction, when a p-type semiconductor is involved a barrier-free ohmic contact is observed at the metal/semiconductor interface, as confirmed by the linear current voltage characteristic obtained for a silver/Merck Lisicon® SP400/silver symmetric junction. This p-type semiconductor was chosen because is a high-performance amorphous polymer. Its polymeric nature permits an easy control over its printability and allows an easy patterning.
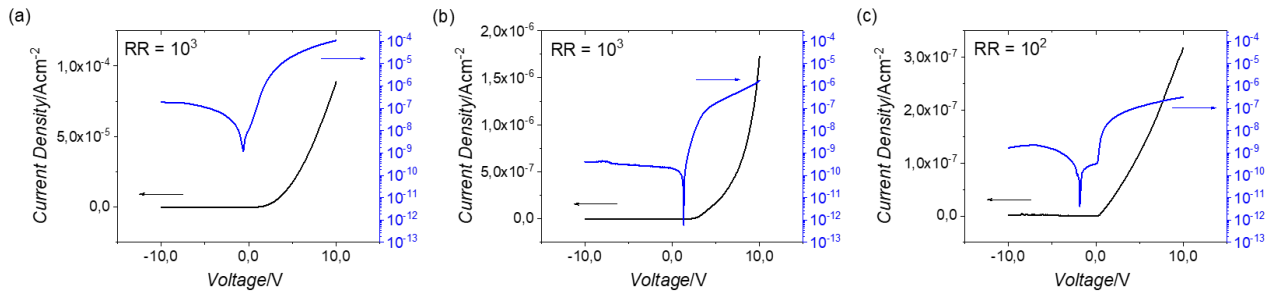
Figure 2 J-V characteristics in linear (left) and semilogarithmic (right) scale for MIS(A) (a), MIS(B) (b), and MIS(C) (c) diodes with drop casted organic semiconductor.

In addition, it reduces its variability because there is no need for a crystallization step [14]. From profile measurements the thickness of the OSC deposited by drop casting was around 500nm.

Thus, a leaky insulator was inserted at the metal/semiconductor interface to obtain a rectifying Barrier Height (BH). Among the family of polymeric dielectrics, the necessity to have an insulator layer with tunable electrical properties makes poly(4-vinylphenol) (PVP) the ideal candidate. Because of this excellent solubility, a wide range of formulations and resulting film thicknesses are possible and most of the PVP formulations have excellent film-forming properties, giving a homogeneous film with a smooth surface [15]. Poly(melamine-co-formaldehyde)methylated was identified as a useful crosslinking agent (CL). By tuning the relative concentration of the polymer and the cross-linker is possible to modulate the resistivity of this material. [16],[17] Three different formulations were investigated: the concentrations of PVP and CL are 50mg/mL and 2.25mg/mL, 90mg/mL and 22.5mg/mL, and 90mg/mL and 45mg/mL in *MIS(A)*, *MIS(B)*, and *MIS(C)*, respectively. Printing parameters were carefully adapted in order to obtain a thickness of the inkjet-printed film of around 1.5μm for all the formulations. The analysis of the electrical characteristics of the MIS diodes was performed on the basis of current density-voltage (J-V) curves. The forward bias corresponds to a positive potential applied to the top silver electrode (silver(f)) with respect to bottom silver electrode (silver(p)). As it can be seen in Figure 2, all the formulations exhibit non-linear, asymmetric, rectifying behaviors thus confirming the introduction of a voltage controlled barrier height at the metal/semiconductor interface due to the presence of the insulating layer. The reverse leakage current and forward current give the indication of the formation of a depletion and accumulation region at the semiconductor/insulator interface, respectively. The Rectification Ratio (RR) is defined as the ratio of the maximum forward bias current to the maximum reverse bias current at the same voltage. At V = |10|V, the Rectification Ratios (RRs) are approximately 10^3 for the formulation A, B and 10^2 for the formulation C. In particular, *MIS(A)* presents a maximum forward current density (J_{f_MAX}) of around 0.1mAcm^{-2} and maximum reverse current (J_{r_MAX}) of around 0.2μAcm^{-2}; *MIS(B)* presents a J_{f_MAX} of around 2.0μAcm^{-2} and J_{r_MAX} 1.2nAcm^{-2}; *MIS(C)* presents a J_{f_MAX} of around 0.7μAcm^{-2} and J_{r_MAX} of around 1.0nAcm^{-2}. From these data, it is evident how the electrical characteristics of the presented diodes are strictly related to the different formulation of the insulating layer, and, as already suggested in our previous work [11], to its interaction with OSC. The relation between the electrical behavior and the cross-linker concentration can be explained through impedance analysis. Table 1 summarizes the electrical parameters obtained for the structures. The impedance and phase angle values were evaluated at a frequency of 1kHz and +5V applied bias. For the lowest cross-linker concentration an impedance value of 6MΩ and a phase of around -60º were measured. These values differ from the ones typical of an ideal MIS capacitor and are responsible for the high reverse leakage current obtained for the *MIS(A)* structure. On the other side, the values obtained for the highest cross-linker concentration reassemble more the ones typical of a variable capacitor, giving a relatively high resistance in forward bias and thus, lowering the RR. The best electrical performances were obtained using the formulation B, which presents a good compromise in terms of impedance and output current.

Table 1. Electrical Parameters of MIS(A), MIS(B), and MIS(C).

MIS	Impedance [MΩ] 1kHz, 5V	Phase [deg] 1KHz, 5V	ε_r	V_t [V]	HB [eV]
A	5.0	-63.5	3.8	0.80	0.18
B	13.4	-77.3	4.7	0.32	0.58
C	17.2	-80.5	4.4	0.32	0.82

Several conduction mechanisms have been proposed to described the conduction trough insulating film. Barrier-limited conduction mechanisms include direct tunneling or Fowler-Nordheim (FN) tunneling and Schottky conduction. Bulk-limited conduction mechanisms include Space-Charge-Limited-Current (SCLC), Poole-Frenkel (PF) conduction, and hopping conduction [18]. Among all, two transport mechanisms mainly occur in this type of structure: the tunneling and the Schottky effect. Depending on the temperature, thickness, and barrier height of the insulating layer, either mechanism predominates. Since this distance changes linearly as a function of the applied voltage, the current varies with the bias voltage. [19] As shown in the *J-V* curves, different slopes were obtained for varied ranges of voltages of the forward voltages, clearly indicating the presence of different transport phenomena in the Ag/cPVP/SP400/Ag structure. All the plots in Figure 3 are referred to MIS(B) structures; however, the same explication can be applied to MIS(A) and MIS(C) diodes. For low-forward bias region (~0.0-0.5V) is possible to observe a plateau in the J-V curves, which is characteristic of a tunneling type conduction. Figure 4a shows a linear dependence of ln(1/V) with 1/V, proper of a Fowler-Nordheim mechanism conduction, with a transition voltage (V_t) of around 0.32V. The same value was obtained for the *MIS(C)*, whilst for the *MIS(A)* V_t = 0.80V.
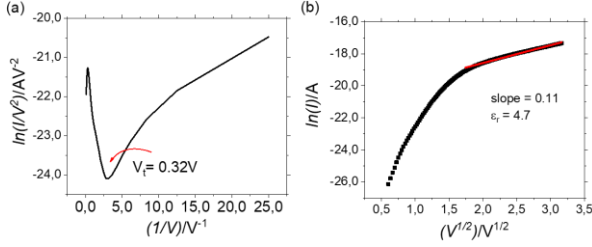
Figure 3 *Ln(I/V^2) vs 1/V fit (a), and Ln(I) vs V$^{1/2}$ fit (b) of MIS(B) structure. In (b) fitting of the linear region were performed and the corresponding slope was utilized to estimate the dielectric constant value.*

Schottky conduction can be described as the field-assisted thermal emission of carriers over the barrier at the metal-insulator interface. Thus, this model was used to confirm the presence of a BH at the metal/semiconductor interface and thus justifying the rectifying behavior. The I-V curves were evaluated using the Schottky equation:

$$\ln(I) = \ln(AA^*T^2) - q\Phi_B/kT + 1/2\beta V^{1/2} \qquad (1)$$

$$\beta = q/KT(q/\pi\varepsilon_0\varepsilon_r L) \qquad (2)$$

where A is the diode area, A^* is the effective Richardson constant, T is the temperature, q is the elementary charge, k is the Boltzmann constant, Φ_B is the BH, ε_0 is the vacuum permittivity, ε_r is the dielectric constant, and L is the insulator thickness. From the slope of the linear fit of ln(I)-V$^{1/2}$ (Figure 3b), a dielectric constant of 4.7 was obtained for cPVP which is in agreement with the literature [ref]. From temperature dependent J-V measurements between 243.15K to 343.15K, it is possible to extract the energy barrier value using the conventional Richardson plot [ref]:

$$\ln(I_0/T^2) = \ln(AA^*) - q\Phi_B/kT \qquad (3)$$

where I_0 is the reverse saturation current derived from the straight line intercept of *ln(I)* at *V*=0V. The slope of the Richardson's plot gives the value of the barrier height. As expected, the highest barrier was obtained for the highest cross-linker concentration. In particular, for MIS(A) structure a BH value of (0.19±0.07)eV, for MIS(B) BH is (0.58±0.12)eV, and for MIS(C) BH is (0.82±0.13)eV.

Once the conduction mechanism was clarified, as a step forward to obtain a totally printed device, the same structures were fabricated depositing the OSC by means of inkjet-printing technique. In this case, the profile thickness of the inkjet-printed OSC was around 150nm. The use of thinner films is desirable to obtain good device electrostatic integrity, resulting
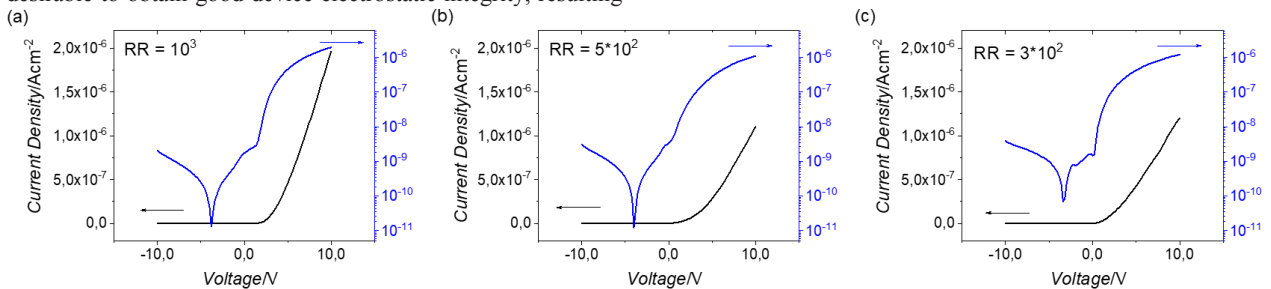
in improved off-state behavior. [14] At a frequency of 1kHz and +5V applied bias, for *MISp(A)* impedance value and phase value were 10.5MΩ and -68.3º, respectively. For *MISp(B)* impedance value and phase value were 12.3MΩ and -70.2º, respectively. For *MISp(C)* impedance value and phase value were 29.7MΩ and -79.0º, respectively. For formulation *A* and *C*, the impedance and phase angle values showed slightly more resistive stacks compared to the ones obtained when the OSC was deposited by drop casting, whilst MISp(B) presented worse performances. These results were confirmed by the *J-V* characteristics shown in Figure 4. Also in this case, the 3 formulations exhibit rectifying behaviors, with a tunneling conduction mechanism clearly recognizable from the plateaus at around 0V. at At V = |10|V, *MISp(A)* and *MISp(C)* present the same RRs obtained for *MIS(A)* and *MIS(C)*: a J_{f_MAX} of around 2.0µAcm^{-2} and 1.0µAcm^{-2} and a J_{r_MAX} of around 2.0nAcm^{-2} and 3.0nAcm^{-2}, respectively. At V = |10|V, *MISp(B)* presents a lower RR with respect to the one obtained for *MIS(B)*, a J_{f_MAX} 1.0µAcm^{-2} and J_{r_MAX} of around 2.0nAcm^{-2}.

Considering these results, *MISp(A)* was chosen to evaluate the possibility of employing the diode structure as a gas sensor.

MIS diode structures as gas sensor

In recent years, many research efforts have been devoted to the development of gas sensors that are able to monitor air pollution. Air quality is an important pre-requisite for public health and its pollution with gaseous compounds contributes relevantly to the burden of disease in both industrial and developing countries. Nitrogen dioxide (NO$_2$), a main pollutant arising from combusted fuel, can cause photochemical smog, acid rains, acute pulmonary, irritation of eyes, and is even suspected to cause cancer. [20] To date, commercial NO$_2$ sensors are usually bulky, have low selectivity, and high power consumption. Even in the most developed cities spatially resolved urban air quality measurements are currently limited. [21] Therefore, it is highly desirable to develop novel gas sensors that are endowed with efficient low cost manufacturing, high throughput, and good device performance such as high sensitivity/selectivity, light weight and low power consumption.

In the past decade, OSC have become promising candidates as materials for gas sensors due to their high sensitivity, low production costs, and multiple function integration. [2] Moreover, the possibility to conduct this analysis at room temperature (RT) is of great importance for operation in complex and often hazardous gaseous environment. [22]

Figure 4 *J-V characteristics in linear (left) and semilogarithmic (right) scale for MISp(A) (a), MISp(B) (b), and MISp(C) (c) MIS diodes with inkjet-printed organic semiconductor.*

The reversible nature of the non-covalent bond interactions between OSCs and gas molecules causes organic materials to be more suitable than inorganic one in the detection of toxic gases such as NO_2, sulfur dioxide (SO_2), or ammonia (NH_3), that may act as either dopants or traps for charge carrier; thus, the interaction processes lead to a change in the charge carrier mobility of the OSCs that can be easily read through the variation of the output signal of an electronic device. An amorphous polymeric semiconductor was chosen to improve the gas diffusion and reduce the problems related to the gas absorption–desorption efficiency typical of OSC characterized by crystal domain boundaries [23].

The setup for the sensing characterization is shown in Figure 5a: the tests were performed on the MISp(A) structure fixed on To-U package (see Experimental). J-V measurements were performed to characterize the electrical response of the MIS diode upon exposure to NO_2 gas. The gas concentration was increased from 1ppm to 100ppm, with an incubation time of 20 minutes before each J-V characterization. As it is shown for 10ppm NO_2 concentration in Figure 5b, after this time the current stabilizes. J-V curves were recorded at ambient condition, during the same period of time, to exclude any possible current variation due to the device instability (Figure 5b, inset).
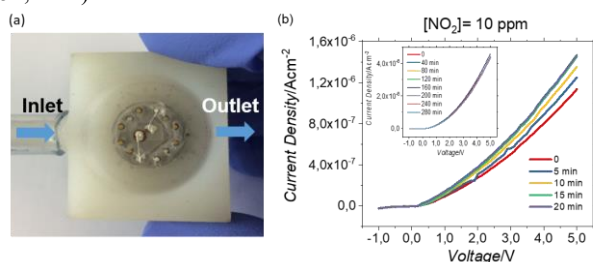
Figure 5 Gas sensing setup (a); variation of the current density of the diode in time after the exposure to 10ppm NO2 concentration (b); stability of the current density signal over 280 minutes (b, inset).

Figure 6a shows the J-V characteristics, registered at room temperature, for the different concentrations of NO_2. The current increases when the concentration of NO_2 is increased: by 7% when the device is exposed to a concentration of the gas of 3 ppm and by 860% when the gas concentration reaches a value of 100 ppm. Being NO_2 a strong electron acceptor species, it generates holes while interacting with a p-type OSC. Therefore, the carrier concentration of semiconductor increases when the diode is exposed to NO_2 gas. The induced carriers firstly fill the traps under the conduction band and then move to the flow current. The charge carrier mobility is dependent on the carrier concentration thus, increasing the carrier concentration, increases the charge carrier mobility, as is clearly visible from the variation of the slope of the *J-V* curves. the relative response intensity The response of the device to NO_2 is shown in Figure 6b was evaluated using the following equation:

$$response = (I_N-I_{N0}/I_{N0})*100 \qquad (4)$$

where I_{N0} and I_N are the maximum forward currents of the sensor recorded in dry air and in presence of NO_2, respectively. From 2ppm to 100ppm the relationship between the response and the NO_2 concentration is non-linear. However, two different linear regions can be distinguished (Figure 7b). From their slopes it is possible to evaluate the device sensitivity: in

the NO_2 concentration range from 2ppm to 10ppm, it is determined to be 11%ppm[-1] (Figure 6c). From 12.5ppm to 100ppm the sensitivity is 9%ppm[-1]. After ceasing the NO_2 flow, the diode conduction decreases correspondingly, and approaches the original current I_{N0}: 120 min was found to be the recovery time of the diode gas sensor. In gas sensing, the selectivity of the sensor is an important factor as well, Figure 6d shows that diodes exhibit a very low sensitivity toward ethanol (EtOH), N_2, and H_2. The investigation and optimization of the device sensing performance in terms of sensitivity (for ultralow concentrations, ppb level) and selectivity will be subject of future studies. However, it is possible to consider this preliminary test as a proof-of-concept of the feasible applications of the presented diodes.
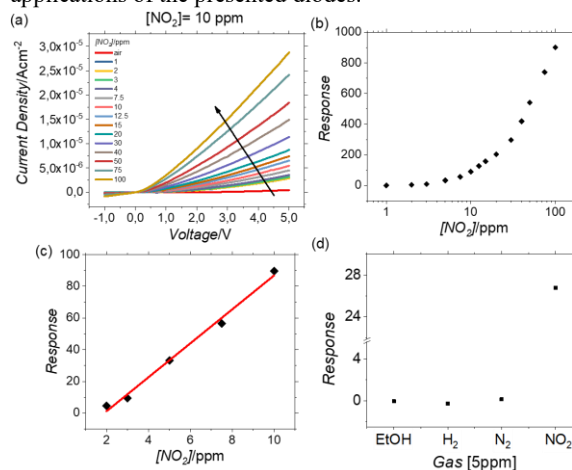
Figure 6 J-V characteristics at room temperature for different concentrations of NO2 (a); response of MISp(a) structure to different concentrations of NO2 (b),(c); device selectivity (d).

Conclusions

In this work, high-performing diodes based on MIS structures were fabricated by inkjet-printing and characterized. Fowler-Nordheim and thermionic emission models were found to be the main conduction mechanisms responsible for carrier injection into the insulator. From temperature-dependent characterizations, is possible to assume that the barrier height at semiconductor/insulator interface depends on the relative concentration of the cross-linker with respect to the polymeric insulator. Best performances were obtained for MIS diodes fabricated using a 25% cross linker concentration, with an energy barrier of 0.58eV and a rectification ratio of around 10^3. The 50% cross linker concentration shows the highest energetic barrier (0.82 eV) and the lower rectifying properties, whilst the 2,5% cross linker concentration shows the lowest energetic barrier (0.18 eV), good rectifying properties but quite high reverse current value. Good electrical performances were obtained, as well, when the organic semiconductor was deposited by inkjet-printing. Finally, a first example of a gas sensor based on the MIS diode is presented as a proof-of-concept for the possible sensing and electronic applications of these structures.

Experimental

MIS diodes were fabricated on 125μm thick Polyethylene naphthalene (PEN) Teonex® Q65HA substrates from Dupont Teijin specially developed for flexible electronics. Substrates were cleaned with subsequent cycles of acetone, isopropyl alcohol, and deionized water, and then dried under nitrogen flow. Before printing the devices, a 40W oxygen plasma treatment (Plasma Technology GmbH) was performed for 20 seconds to increase wettability of substrates. A Fujifilm Dimatix DMP2831 desktop printer was used as the printing setup. The silver conductive ink used for the bottom silver(p) electrodes is a 30% solid content ink (DGP-40LT-15C, ANP). A drop spacing (DS) of 20 μm was employed and the printer platen was kept at 40ºC. Finally, the patterned layer was sintered at 120ºC for 30 min in a convection oven. Three different solution of poly(4-vinylphenol) (PVP) using poly(melamine-co-formaldehyde) methylated as crosslinking agent (CL) in propylene glycol methyl ether acetate (PGMEA) were used as insulators layers. The concentrations of PVP and CL are 90 mg/mL and 45 mg/mL, 90mg/mL and 22.5mg/mL, and 50mg/mL and 2.25mg/mL in solution A, B, and C, respectively. The dielectric layer was inkjet-printed using a DS of 30 μm and keeping the substrate at room temperature. Cross-linking was performed on a convection oven for 30 minutes at 150°C; cross-linking step was performed after each layer deposition. The organic semiconductor is a commercial amorphous p-type semiconductor (Lisicon® SP400, Merck) and it was deposited on the top of the dielectric layer using drop casting and inkjet- printing technique. thermally. The OSC layer was inkjet-printed using a DS of 15 μm, keeping the substrate at room temperature. For both the deposition techniques, the curing process was performed on a hot plate for 2 minutes at 100ºC. The top silver(f) electrode is silver conductive paste from Electrolube and it was deposited by means of drop casting technique and dried in air.

All the fabrication processes and electrical measurements were performed in ambient conditions and ambient light. The MIS structure IV characterizations were carried out using an Agilent B1500A semiconductor parameter analyzer. Capacitive measurements were performed with an Agilent E4980A LCR meter and Keithley 4200 semiconductor parameter analyzer. The images were acquired using a light microscope DM4000 from Leica. The layer thickness for the dielectric layers were evaluated using a mechanical surface Dektak profilometer. Atomic Force Microscopy images were carried out using the Nanoscope Veeco Dimension 3100. The response of the diodes towards nitrogen dioxide was recorded using a homemade stainless steel chamber of 8.6 mL volume connected to a Gometrics MGP2 gas mixer with four Bronkhorst Mass-Flow Controllers. Electrical measurements, carried on with Keithley 2602A dual source measure units, and flowing gas concentrations were controlled using self-developed Labview software. For all the gas measurements, a constant flow of 200 mL/min was kept.

References

[1] J. S. Chang, A. F. Facchetti, R. Reuss, IEEE Trans. Emerg. Sel. Topics Circuits Syst., 7, 7 (2017).

[2] Jolke Perelaer, Ulrich Sigmar Schubert, Polymer Science: A Comprehensive Reference (Elsevier, Oxford, UK, 2012), pg 167.

[3] Hagen Klauk, Organic Electronics II (Wiley-VCH Verlag GmbH & Co. KGaA, Weinheim, Germany, 2012), pg 281.

[4] A. Salim, S. Lim, Sensors, 17, 2593 (2017).

[5] J. Noh, M. Jung, Y. Jung, C. Yeom, M. Pyo, G. Cho, Key Issues With Printed Flexible Thin Film Transistors and Their Application in Disposable RF Sensors, Proc. IEEE, pg. 554 (2015).

[6] X. Peng, J. Yuan, S. Shen, M. Gao, A. S. R. Chesman, H. Yin, J. Cheng, Q. Zhang, D. Angm, Adv. Funct. Mater., 27, 1703704 (2017).

[7] E. Ramon, C. Martínez-Domingo, A. Alcalde-Aragonés, and J. Carrabina, IEEE Trans. Emerg. Sel. Topics Circuits Syst, 7, 161 (2017).

[8] T. M. Kraft, P. R. Berger, D. Lupo, Flex. Print. Electron., 2, 033001 (2017).

[9] H.-L. Yip, A. K.-Y. Jen, Energy Environ Sci., 5, 5994 (2012).

[10] K. E. Lilja, H. S. Majumdar, F. S. Petterson, R. Österbacka, T. Joutsenoja, ACS Appl. Mater. Interfaces, 3, 7 (2011).

[11] K. Y. Mitra, C. Sternkiker, C. Martínez-Domingo, E. Sowade, E. Ramon, J. Carrabina, H. L. Gomes, R. R. Baumann, Flex. Print. Electron., 2, 015003 (2017).

[12] D. Tobjörk, N.J. Kaihovirta, T. Mäkela, F.S. Pettersson, R. Österbacka, Organic Electronics, 9, 931 (2008).

[13] A.M. Nardes, M. Kemerink, M.M. de Kok, E. Vinken, K. Maturova, R.A.J. Janssen, 9, 727 (2008).

[14] G. Grau, V. Subramanian, Adv. Electron. Mater., 2, 1500328 (2016).

[15] Hagen Klauk, Organic Electronics, Materials, Manufacturing and Applications, (Wiley-VCH Verlag GmbH & Co. KGaA, Weinheim, Germany, 2006) pg.

[16] M.E. Roberts, N. Queraltò, S.C.B. Mannsfeld, B.N. Reinecke, W. Knoll, Z. Bao, Chem. Mater., 21, 2292 (2009).

[17] S. Conti, S. Lai, P. Cosseddu, A. Bonfiglio, Adv. Mater. Technol., 2, 1600212 (2017).

[18] T.W. Hickmott, J. Appl. Phys. 97, 104505 (2005).

[19] S. Hemour, K. Wu, Radio-Frequency Rectifier for Electromagnetic Energy Harvesting: Development Path and Future Outlook, Proc. IEEE, pg. 1667 (2014).

[20] K. Wetchakun, T. Samerjai, N. Tamaekong, C. Liewhiran, C. Siriwong, V. Kruefu, A. Wisitsoraat, A. Tuantranont, S. Phanichphant, Sens. Actuator B-Chem., 160, 580 (2011).

[21] A. R. Jalil, H. Chang, V. K. Bandari, P. Robaschik, J. Zhang, P. F. Siles, G. Li, D. Bürger, D. Grimm, X. Liu, G. Salvan, D. R. T. Zahn, F. Zhu, H. Wang, D. Yan, O. G. Schmidt, Adv. Mater., 28, 2971 (2016).

[22] C. Zhang, P. Chen, W. Hu, Chem. Soc. Rev., 44, 2087 (2015).

[23] A. Lv, Y. Pan, L. Chi, Sensors, 17, 213 (2017).

Author Biography

Silvia Conti received her M.Sc. in Industrial Chemistry in 2013. In 2017 she defended her Doctoral Thesis "Fully printed Organic Thin Film Transistors for Biosensing Applications" in Bioengineering and Robotic under the supervision of Professor Annalisa Bonfiglio. She is currently enrolled in the Integrated Circuit & System (ICAS) group of IMB-CNM (CSIC) in Barcelona as a Post-Doctoral Researcher. Her research activity is focused on the fabrication of organic semiconductor devices by using the inkjet-printing technique.